Iran J Sci Technol Trans Sci (2021) 45:885–898
https://doi.org/10.1007/s40995-021-01103-6

RESEARCH PAPER

Direct Impregnation of MgO Nanoparticles in 58S Bioactive Glass: Bioactivity Evaluation and Antibacterial Activity

Seyed Peiman Ghorbanzade Zaferani[1] · Nima Nabian[1] · Maedeh Delavar[1] · Sayed Mahmood Rabiee[2]

Received: 25 August 2020 / Accepted: 26 February 2021 / Published online: 24 March 2021

Abstract
Bioactive glasses are recognized as the favorable biomaterials in bone tissue engineering. In this study, novel bioactive nanocomposites based on 58S bioactive glass in composite with various weight percent of magnesium oxide nanoparticles were prepared. The bioactivity of nanocomposite powders was evaluated through immersion of samples in the simulated body fluid (SBF) at different time intervals of 14 and 28 days. Moreover, the nanocomposite samples were characterized in terms of morphology, phase structure and functional groups using scanning electron microscopy, X-ray diffraction and Fourier transform infrared spectroscopy (FTIR) before and after soaking in the SBF solution. It was found that hydroxyapatite was formed on the surface of all nanocomposites after soaking in the SBF solution, although the bioactivity decreased with an increase in the amount of MgO nanoparticles from 15 to 25 wt%. Moreover, antibacterial activity of the produced nanocomposites against MRSA bacteria was investigated and the results showed that 58S-15 Mg exhibited the highest bactericidal activity.

Keywords 58S-MgO bioactive nanocomposites · Bioactivity evaluation · Antibacterial activity · MRSA bacteria

1 Introduction

For more than half of a century, many studies have been conducted in order to find a reasonable candidate for the reconstruction and repair of the defective bone tissues which were mainly caused by accidental injuries and various bone illnesses such as tumors, trauma or infection (Osteomyelitis) (Strobel et al. 2013; Ye et al. 2019). One of the main strategies proposed to eliminate these bone defects has been the application of a variety of biological materials such as ceramic-based implants and scaffolds. Bioceramics are synthetic materials with excellent biocompatibility toward living tissue and therefore can be used in medicine to repair defects and replace damaged tissues (Abdalla et al. 2020; Shih et al. 2013).

Among the bioceramics, bioactive glasses (BGs) are recognized as the favorable biomaterials in the field of bone tissue engineering since they can quickly form a bond with both hard and soft tissues (Cole et al. 2019; Shih et al. 2012). The capability of BGs in the formation of a bone bonding was investigated in many researches in which the researchers located the bioactive glasses in contact with the biological media. They have reported that the main reason for the bonding ability was the creation of a hydroxyapatite (HA) layer at the interfacial surface of bioactive glasses and the biological fluids (Rabiee et al. 2015; Sukhorukova et al. 2017; Sun et al. 2019).

It is known that Prof. Larry Hench was the inventor of bioactive glasses, who synthesized the first ones using the melt-quenching process in 1969 at the University of Florida. Later, his fabricated bioactive glass was named 45S5 Bioglass® due to its composition in weight percent (45% SiO_2, 24.5% CaO, 24.5% Na_2O and 6% P_2O_5) (Kaur et al. 2016a). Another technique for the preparation of bioactive glasses was presented in 1991 by Li et al. (1991) that named as the sol–gel method. This bottom-up procedure is

✉ Nima Nabian
nimanabian@mazust.ac.ir

[1] Department of Chemical Engineering, University of Science and Technology of Mazandaran, P.O. Box, 48518-78195 Behshahr, Iran

[2] Department of Materials Engineering, Babol Noshirvani University of Technology, P.O. Box, 47148-71167 Babol, Iran

done at considerably lower temperatures compared to conventional melt-quenching and constitutes two key reactions of glass precursors, namely hydrolysis and condensation (Lucas-Girot et al. 2011).

Sol–gel-derived inherently porous bioactive glasses can be synthesized in different morphologies among which the nanoparticles have attracted the particular attention of many researchers due to their premium features like great specific surface area and small particle size (dos Santos et al. 2019; Farano et al. 2019). In fact, the larger specific surface area of nano-sized bioactive glasses compared to that of microparticles may lead to the enhancement in the hydroxyapatite deposition process and also the formation of tighter bone bonding because more active sites at the interface will be present for osteoblast to attach (Hong et al. 2019; Huang et al. 2018).

It can be found in the literature that some researchers incorporated different metal oxides (MO) like calcium oxide, zinc oxide and magnesium oxide in the structure of SiO_2–CaO–P_2O_5-based bioactive glasses and fabricated BG-MO nanocomposites to enhance the bioactivity and antibacterial activity of sol–gel-derived bioactive glass nanoparticles (Liu et al. 2018; Mohammadkhah and Day 2018; Sawai 2003). Due to the significant function of magnesium element in the human bone metabolism, such as osteoblast differentiation and osteogenic gene expression (Feyerabend et al. 2006; Yoshizawa et al. 2014), these element-based oxides are considered as an appropriate alternative to be applied in the structure of bioactive glasses for the improvement of bioactivity.

It is worth mentioning that magnesium oxide has been incorporated in the preparation of bioactive glasses in different ways. In most of those studies, magnesium oxide (MgO) was usually added, as a new component to the composition of common ternary (SiO_2–CaO–P_2O_5), (Gu et al. 2019; Ma et al. 2010a, 2011b; Moghanian et al. 2018b; Pérez-Pariente et al. 2000; Prabhu et al. 2013) or quaternary (SiO_2–Na_2O-CaO–P_2O_5), (Aguiar et al. 2008; Kaur et al. 2016b; Li et al. 2013) bioactive glasses. In these surveys, the researchers used some sources for MgO like magnesium nitrate hexahydrate in the composition of bioactive glasses and did not use MgO directly as a starting material in sol–gel method. In fact, magnesium oxide was substituted for one of the main constituents (usually calcium oxide) in the formula of bioactive glasses like 58S ($58SiO_2$–$33CaO$–$9P_2O_5$ (wt%)). For instance, Prabhu et al. (2013) decreased the weight percent of CaO and instead added MgO with the weight percent of 10 and 20 to the aforementioned composition of 58S so that the obtained $58SiO_2$–$23CaO$–$9P_2O_5$–$10MgO$ and $58SiO_2$–$13CaO$–$9P_2O_5$–$20MgO$ nanobioactive glasses exhibited better in vitro bioactivity compared to common 58S and did not reveal significant antibacterial activity. In another work (Moghanian et al. 2018b), the molar composition of CaO was changed by the addition of a different mole percent of MgO in the range of 0–10. In that survey, it was revealed that the bioactivity of synthesized bioactive glasses was first increased with an increase in mole percent of MgO and then decreased so that the composition of $60SiO_24P_2$-$O_531CaO5MgO$ (mole %) had the highest formation rate of hydroxyapatite. Also, the antibacterial activity of the samples was investigated against methicillin-resistant staphylococcus aureus (MRSA bacteria) which is the major clinical-acquired type of Staphylococcus aureus infection and also shows resistance to some antibiotics (Moghanian et al. 2018b).

In another point of view, some researchers have focused on the direct incorporation of metal oxide nanoparticles into bioglass and fabricated bioactive glass–metal oxide nanocomposites due to the great characteristics of nanobioactive glasses, such as great antibacterial behavior, (Seuss et al. 2014) osteoblast cell adhesion and proliferation (Taherian et al. 2014). As an example, Saqaie et al. (2016) synthesized bioactive glass–forsterite nanocomposites by adding the various weight percent of forsterite (Mg_2SiO_4) to the 58S bioactive glass powders and studied its effect on the bioactivity of the prepared samples. They concluded that the sample containing 20 wt% of forsterite exhibited the highest bioactivity by the formation of a hydroxyl-carbonate apatite layer (HCA) on the nanocomposite surface.

According to above-mentioned explanations, it is clear that different results were reported on the effect of the MgO contents in bioglass composition on the in vitro rate of HA formation (Bellucci et al. 2017; Ma et al. 2010b). It can be found that the previous studies have focused on the incorporation of MgO sources like $Mg(NO_3)_2.6H_2O$ by decreasing the percentage of other precursors involved in the synthesis of 58S bioactive glass, while it could be attractive to evaluate the variations in the bioactivity of samples through addition of MgO without changing the routine composition of 58S bioactive glass. Moreover, to the best of our knowledge, there is no research reporting the effect of direct impregnation of MgO nanoparticles, with a good number of active sites for HA nucleation, into 58S bioactive glass on the bioactivity of resulting nanocomposites. The main goal of this research is to prepare a novel bioactive glass–magnesium oxide nanocomposite by impregnating different weight percent of magnesium oxide nanoparticles directly into 58S bioactive glass material. Moreover, the effect of MgO nanoparticles content present in the nanocomposites structure on the bioactivity of nanocomposite powders was evaluated through immersion of samples in the simulated body fluid at different time intervals of 14 and 28 days. Finally, the nanocomposite sample with the highest bioactivity was

determined by comparing the bioactivity results obtained from characterization tests. Moreover, antibacterial activity of the produced bioactive nanocomposites against methicillin-resistant Staphylococcus aureus (MRSA) bacteria is investigated. Then, the antibacterial activity of the nanocomposites containing magnesium oxide nanoparticles was compared together to find best sample in this regard.

2 Materials and Methods

2.1 Reagents

The sol–gel precursors used in this study were tetraethyl orthosilicate (TEOS: $Si(OC_2H_5)_4$), triethyl phosphate (TEP: $(C_2H_5)_3PO_4$), calcium nitrate tetrahydrate (CN: $Ca(NO_3)_2.4H_2O$), ammonia (NH_3) and nitric acid (HNO_3). The molarities of ammonia and nitric acid used in this study were 1 M and 2 M, respectively. All chemicals were used without further purification and purchased from Merck, Germany.

2.2 Synthesis of 58S Nanobioactive Glass.

In this work, the composition selected for the preparation of bare bioactive glass was 58S (Nabian et al. 2013). The first step procedure involved mixing TEOS, distilled water and HNO3 in order. Ethanol as an alcoholic medium was added to the solution and allowed to react for 30 min for the acid hydrolysis of TEOS to proceed almost to completion. The following reagents were added in sequence allowing 20 min for each reagent to react completely: TEP, $Ca(NO_3)_2.4H_2O$, ammonia solution. After the final addition, mixing was continued until the gel was formed. The gel was kept in the oven and heated at 60 °C for 1 day to remove the residual water and ethanol. Then, the dried sample was calcined for two hours at 600 °C with the heating rate of 3 °C/min to stabilize the glass and eliminate residual nitrate (sample 58S).

2.3 Synthesis of 58S-xMgO Bioactive Nanocomposites

In order to synthesize bioactive nanocomposites consisting of 58S bioactive glass and magnesium oxide nanoparticles, the sequence of adding precursors was similar to that described in the previous section until the addition of CA $(NO_3)_2.4H_2O$. Afterward, MgO nanopowders with various weight ratio (MgO to 58S bioactive glass), of 0.05, 0.15 and 0.25 (5%, 15% and 25%) were added to the solution. Then, mixing was continued until the gel was formed. Finally, the gel was dried and calcined at the same conditions as mentioned in the previous section. The attained samples are hereafter referred as 58S-xMg samples (Table 1) where x represents weight fraction of MgO nanopowder in the synthesized composite (x = 5, 15, and 25).

2.4 Characterization of the Samples

A phase structure evaluation was performed by the XRD technique using X-ray diffractometer (XRD, EQUINOX 3000, USA), with CuKα over 2θ range of 10–80° with step size of 0.032° in the fixed time mode, to improve the count statistics. The diffraction patterns were analyzed using the Rietveld structure refinement method as implemented in High Score Plus software. All of the cif files used in this study were identified by the American Mineralogist Crystal Structure Database (AMCSD) codes. The morphological studies of the prepared powders were carried out using scanning electron microscopy (SEM, EM3200, China) working at 30 kV as well as transmission electron microscopy (TEM 208S). Analysis and determination of the functional groups of the samples were performed by Fourier transform infrared spectroscopy (FTIR, Bomem, MB-100, USA) using KBr pellets technique in the range of 400–4000 cm^{-1}. Dynamic light scattering (DLS) was carried out for particle size analysis. DLS is a technique for determining particle size in colloidal suspensions. It often referred to as photon correlation spectroscopy (PCS). In this study, DLS test was done by Malvern Zetasizer NANO ZSP ZEN-5600. The laser wavelength, detection angle and laser output are 633 nm (He–Ne laser), 173° and 4.0 mW, respectively. The viscosity of the brine is selected as water to be 0.8872 cP. The refractive indices of dispersant and material are taken to be 1.33 and 1.59, respectively (Hoo et al. 2008).

2.5 In-vitro Bioactivity Analysis

The corrected Kokubo's simulated body fluid (SBF) (Bohner and Lemaitre 2009), with ion concentrations similar to that of human blood plasma was applied for in vitro bioactivity assessment of the prepared nanopowders. The samples (58S, 58S-5MgO, 58S-15MgO and 58S-25MgO) with a concentration of 25 mg/ml were immersed

Table 1 Chemical compositions of synthesized samples

Sample	Matrix (weight. %)			Reinforcement (weight fraction)
	SiO_2	CaO	P_2O_5	MgO
58S	58	33	9	0
58S-5 Mg	58	33	9	0.05
58S-15 Mg	58	33	9	0.15
58S-25 Mg	58	33	9	0.25

in the SBF solution for 14 and 28 days. During the test, the solution was kept at around physiological temperature in the incubator. At the end of the 14th and 28th days of soaking in the SBF, the solutions were washed with deionized water and then kept at room temperature until dry.

2.6 Antibacterial Test

The antibacterial activity of bioactive glasses against MRSA was achieved to investigate the effect of Mg on antibacterial activities in prepared samples. Thus, MRSA was cultured in liquid lysogeny broth (LB) medium at 37 °C and was diluted approximately to 0.5×10^8 to 2×10^8 ml^{-1} prior to the experiment. First, 10 mg of each bioactive glass powder and 0.9 ml LB medium were added to 1.5-ml Eppendorf tube followed by stirring for 1 min. Then, 0.1 ml bacterial suspension was added into each Eppendorf tube and the solutions were cultured at 37 °C for 1 h. After a serial dilution, 100 μl suspensions were plated onto LB-agar plates and incubated overnight at 37 °C in the dark (Moghanian et al. 2018a). The bactericidal percentage were calculated by counting the final colony-forming units per milliliter (CFU/ml) as follows:

$$Bactericidal\,fraction = 1 - (number\,of\,survived\,bacteria/number\,of\,total\,bacteria).$$

3 Results and Discussions

In this section, the interpretation of the acquired results is discussed in two main subsections; in the first one, the characterization data obtained from 58S nanobioactive glass before and after immersion in the simulated body fluid are discussed while the second subsection describes those gained for 58S-xMg samples in the same experiments.

3.1 58S Nanobioactive Glass

3.1.1 Particle Size Analysis

The particle size distribution of 58S bioactive glass based on the number is presented in Fig. 1 using the DLS analysis. A detailed description of the DLS results represented that 98.1% of glass particles possessed the particle size between 70 and 200 nm. Moreover, it has been found that more than 80% of the particles were in the range of 70 to 122 nm. The reason for the presence of some particles with larger sizes could be the inadequate dispersion of the synthesized particles in the solution required for DLS measurements. Because of nanobioactive glasses have a higher specific surface area compared to micro-sized, from DLS test, it will expect that the synthesized composites will show good biological properties (Wang et al. 2020).

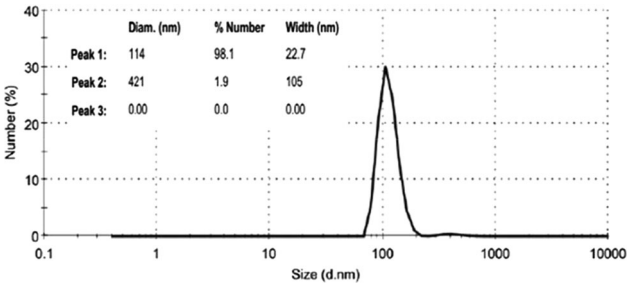

Fig. 1 The DLS analysis of 58S nanobioactive glass

3.1.2 Surface Morphology Analysis

TEM image of 58S nanobioactive glass is displayed in Fig. 2. It can be realized that the sizes of synthesized particles were below 200 nm which is in good agreement with the DLS results. Figure 3 shows the SEM images of 58S nanobioactive glass before and after immersion in the SBF for 14 and 28 days. As it is clear from these figures, there was a difference between the morphology of the samples before and after immersion in the SBF. The resulting morphology before immersion indicated the presence of spherical particles. However, it can be seen that new particles have been formed on the 58S bioactive glass after immersion in simulated body fluid, which could be related to the formation of hydroxyapatite on the sample. This change in morphology is in consistency with the results obtained by Taghian et al. (2015) who regarded the

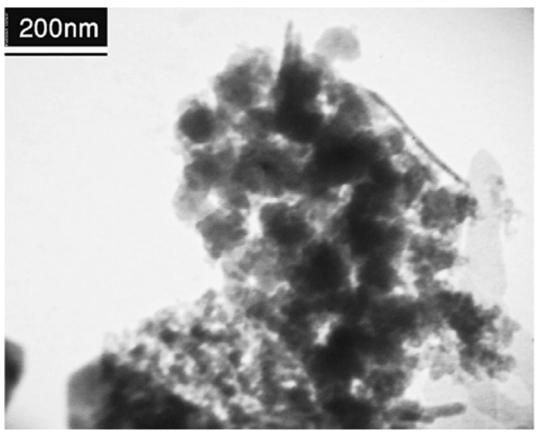

Fig. 2 TEM image of synthesized 58S bioactive glass

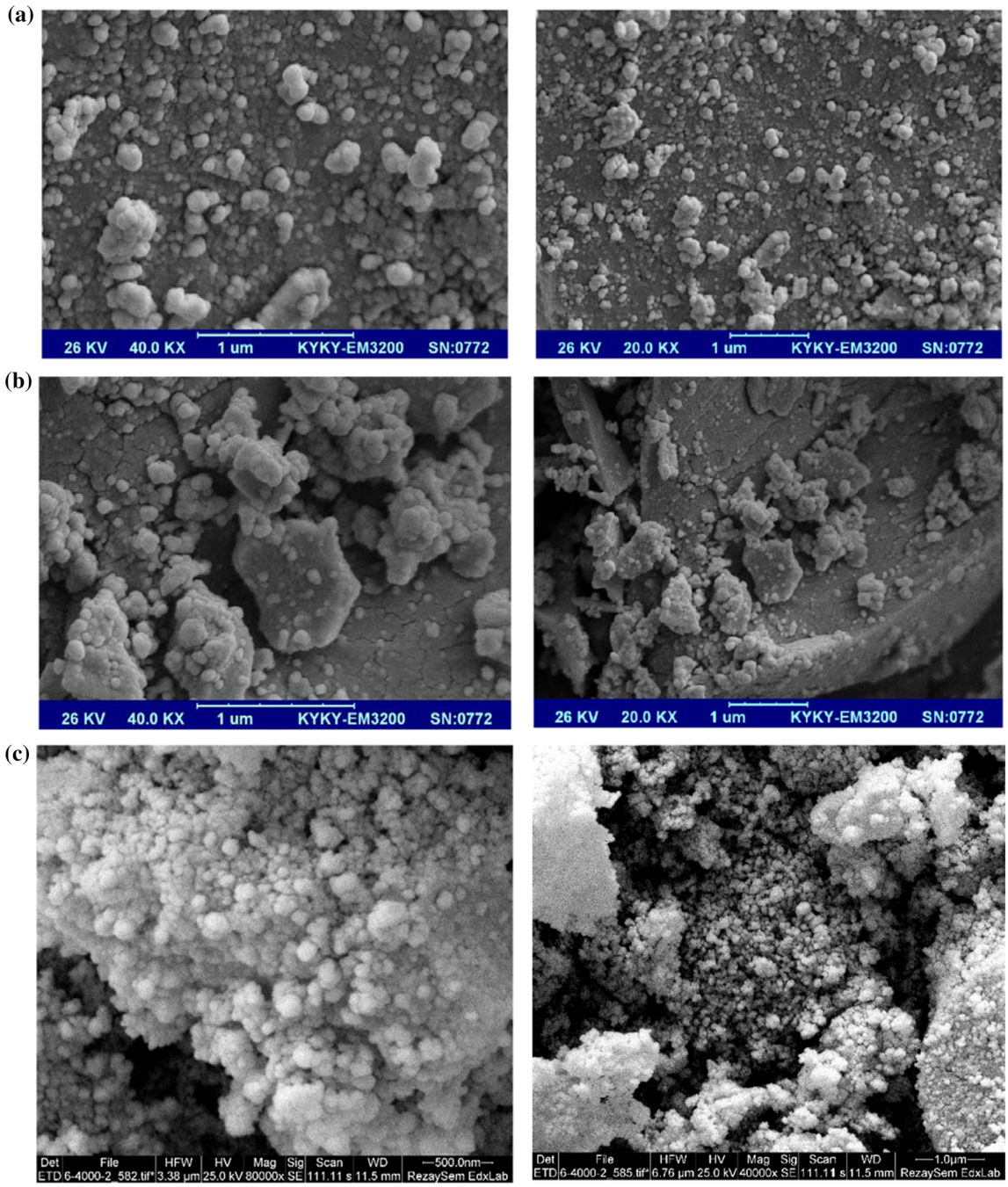

Fig. 3 SEM images of 58S bioactive glass at different resolutions **a** before, **b** after 14 days and **c** after 28 days of immersion in the SBF

dissolution–deposition process and the formation of hydroxycarbonate apatite (HCA) as the reason for the morphological change. It is worth mentioning that the presence and formation of hydroxyapatite require further investigation using XRD analysis. According to the SEM images, it can also be concluded that with an increase in the immersion time of the samples in the SBF, the formation of hydroxyapatite clusters was also enhanced.

3.1.3 Phase Structure Analysis

The X-ray diffraction pattern of 58S nanobioactive glass powders is observed in Fig. 4. The amorphous or glassy nature of the synthesized 58S sample is confirmed by the resulted broad peaks and the absence of sharp ones. Indeed, the formation of the Si–O–Si network has been proven by the broad peaks appeared in the XRD image of the sample

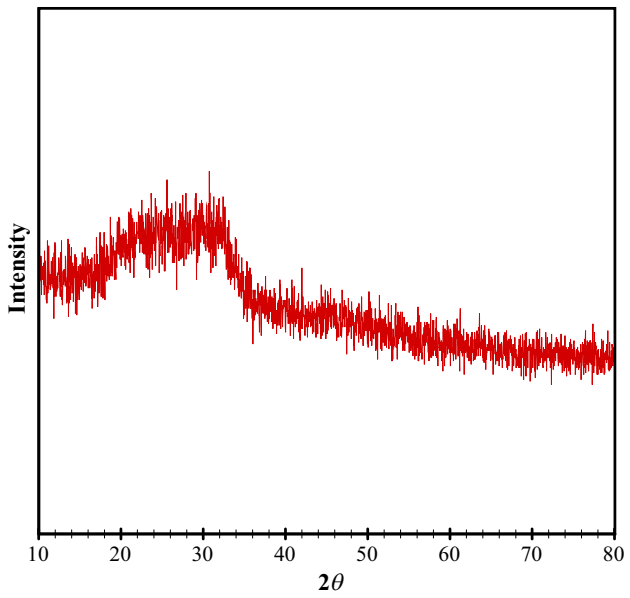

Fig. 4 XRD pattern of 58S nanobioactive glass

in the 2-theta angle range of around 18 to 34 degrees (Zhou et al. 2012). Moreover, this pattern is in good agreement with the XRD pattern of 58S bioactive glasses prepared by Saravanakumar et al. (2015).

The X-ray diffraction patterns of 58S nanoglass before and after 14 and 28 days of immersion in the SBF solution are presented in Fig. 5. By evaluating the XRD patterns before and after immersion, it is evident that some new peaks were appeared in the XRD image of the sample after

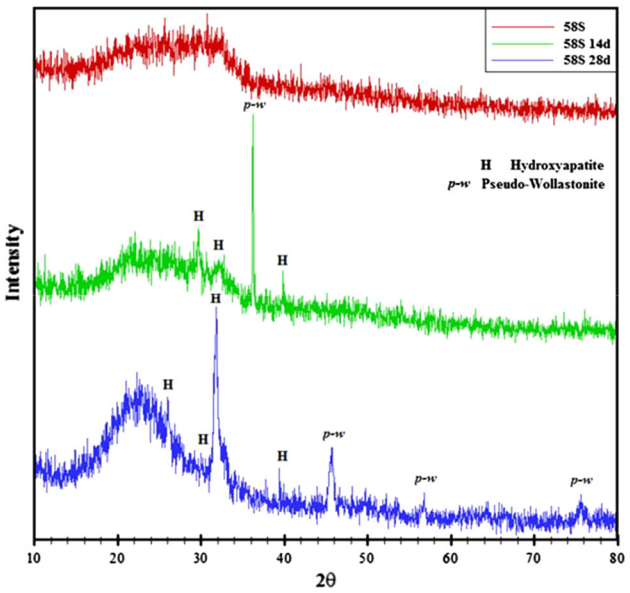

Fig. 5 XRD patterns of 58S nanobioactive glass before (58S sample- upper pattern), after 14 days (58S-14d sample- middle pattern) and 28 days (58S-28d sample- down pattern) of immersion in the SBF solution

immersion compared to that of before immersion. Peaks at approximately 24° (111), 26° (002), 30° (210), 32° (211) and 39° (310) (Anand et al. 2014; Saboori et al. 2009), angles indicated the presence of the hydroxyapatite phase, on the surface of the sample during in vitro test, according to the card number of 0432–9 based on the Joint Committee on Powder Diffraction Standards (JCPDS). Also, peaks at about angles of 36, 46, 56 and 76 degrees, according to the American Mineralogist Crystal Structure Database (AMCSD) standard number of 0,002,247, represent the pseudowollastonite phase which has been regarded as a bioactive material (Mokhtari et al. 2018; Rabiee et al. 2018). As can be realized from these patterns, increasing the time duration of immersion of 58S nanobioactive glass in the SBF solution, its bioactivity increases concerning the intensity and appearance of hydroxyapatite phase peaks. Accordingly, it can be perceived that the sample immersed in the SBF solution for 28 days, exhibited the highest bioactivity. Also, Tables 2 and 3 show details of XRD patterns for 58S-14d and 58S-28d bioactive samples, respectively.

3.1.4 Functional Groups Analysis

The FTIR spectra of the 58S nanobioactive glass powders before and after immersion in the SBF solution for 14 and 28 days are displayed in Fig. 6. The peak observed at the wavenumber of 1090 cm^{-1} can be related to the asymmetric stretching bond of the Si–O–Si (Saqaei et al. 2016). Obviously, some new peaks have been emerged in the FTIR spectra of 58S nanobioactive glass after exposure to the SBF solution. The appearance of a peak at a wavenumber of about 470 cm^{-1} in the bioactive glass sample after immersion in the SBF can be attributed to the vibrating phosphate bond (P-O) present in the crystalline apatite layer on the surface of the specimens (Taghian Dehaghani et al. 2015). Besides, the peak at 1090 cm^{-1} became sharper, which can be imputed to the destruction of the Si–O–Si network to form hydroxyapatite. This reasoning can be understood from the available typical absorption band of hydroxyapatite seen in the wavenumber area of 910–1040 cm^{-1} attributed to υ_3 PO_4 (Ji et al. 2017). Also, peaks corresponding to the wavenumbers of 603 and 565 cm^{-1} represent the P-O bond in υ_4 PO_4 in the apatite network (Taghian Dehaghani et al. 2015). The peak at 800 cm^{-1} is related to the symmetric stretching vibration of Si–O–Si (Nabian et al. 2011). Two other visible peaks at the wavenumbers of 1651 and 3500 cm^{-1} can be ascribed to the tensile vibrations of O–H in the Si–OH groups due to the absorption of water in the solution. This indicates that the glass surface possessed a large number of silanol groups (Huang et al. 2014). The presence of water may be due to the presence of strong nucleophilic groups such as

Table 2 Details of XRD pattern for bioactive materials phase – 58S-14d

Peak position 2θ (°)	FWHM Bsize (°)	d-spacing (A°)	Dp (nm)	Dp average (nm)
24.2	2	3.67869	4.25	6.45
29.69	1	3.01412	8.59	
32.26	2	2.77525	4.32	
39.88	0.8	2.26082	11.04	
26.1	2.1	3.41617	4.06	

Table 3 Details of XRD pattern for bioactive materials phase – 58S-28d

Peak position 2θ (°)	FWHM Bsize (°)	d-spacing (A°)	Dp (nm)	Dp average (nm)
22.12	3.2	4.02535	2.644022	10.74626728
25.81	1	3.45701	8.518897	
31.839	0.48	2.81077	17.9894	
39.6	0.9	2.27677	9.80609	
45.72	0.61	1.98773	14.773	

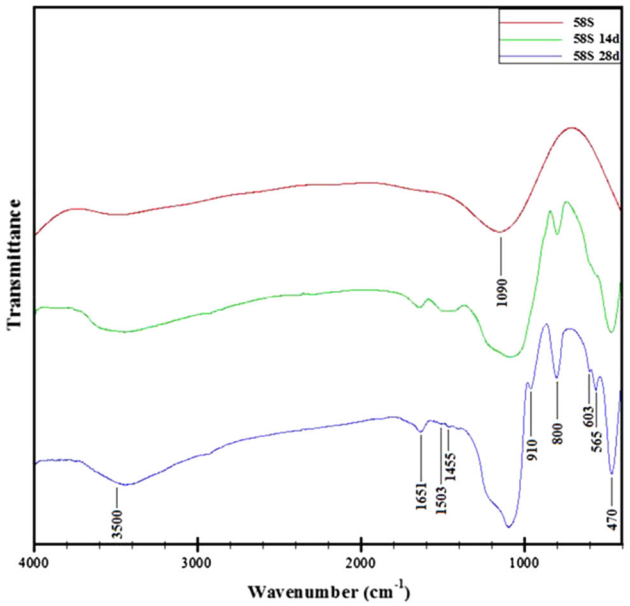

Fig. 6 FTIR spectra of 58S nanobioactive glass before (58S sample- upper pattern), after 14 days (58S-14d sample- middle pattern) and 28 days (58S-28d sample- down pattern) of immersion in SBF solution

P-OH or Ca-OH, which has led to moisture absorption (Mami et al. 2008). The peak occurred at 1503 cm^{-1} is related to carbonate bonds in hydroxyapatite (Deng et al. 2014). Also, the peak at the wavenumber of about 1455 cm^{-1} is related to the C-O bond in the carbonate groups substituted for phosphate groups in the apatite network (Rainer et al. 2008). It should be noted that these results are verified by the findings reported by Moghanian et al. (2018a) Regarding the intensity of the peaks corresponding to the hydroxyapatite phase, it can be concluded that the 58S sample with the highest bioactivity was obtained after 28 days of soaking in the SBF.

3.2 58S/x-Mg Nanocomposites

In this section, the characterization data of the prepared nanocomposites, containing 58S bioactive glass and different amounts of magnesium oxide nanoparticles, obtained before and after immersion in the SBF were demonstrated and also compared with those characterization data represented in the previous section for 58S nanobioactive glass.

3.2.1 Surface Morphology Analysis

Figure 7 shows the SEM images of the 58S-25 Mg nanocomposite before and after soaking in the simulated body fluid for 14 and 28 days. As displayed in Fig. 7a, the synthesized nanocomposite possessed spherical nanoparticles. Furthermore, based on the pictures taken from this sample after 14 (Fig. 7b) and 28 days (Fig. 7c) of soaking in the SBF solution, it is observed that hydroxyapatite clusters were formed on the sample. It can be proven that bioactive glass with spherical particles exhibits superior biological activity due to regular shape (Wang et al. 2020). Also, it can be seen that more clusters were present on the surface of the sample after 28-day immersion. The reason for this phenomenon can be this matter that as the days of soaking increased from 14 to 28, the nuclei created by apatite were grown as well and then distributed throughout the sample so that they covered almost an array of sites on the surface of the prepared nanocomposite (Moghanian et al. 2018a).

3.2.2 Phase structure analysis

The x-ray diffraction patterns of 58S-5 Mg, 58S-15 Mg and 58S-25 Mg bioactive nanocomposites are illustrated in

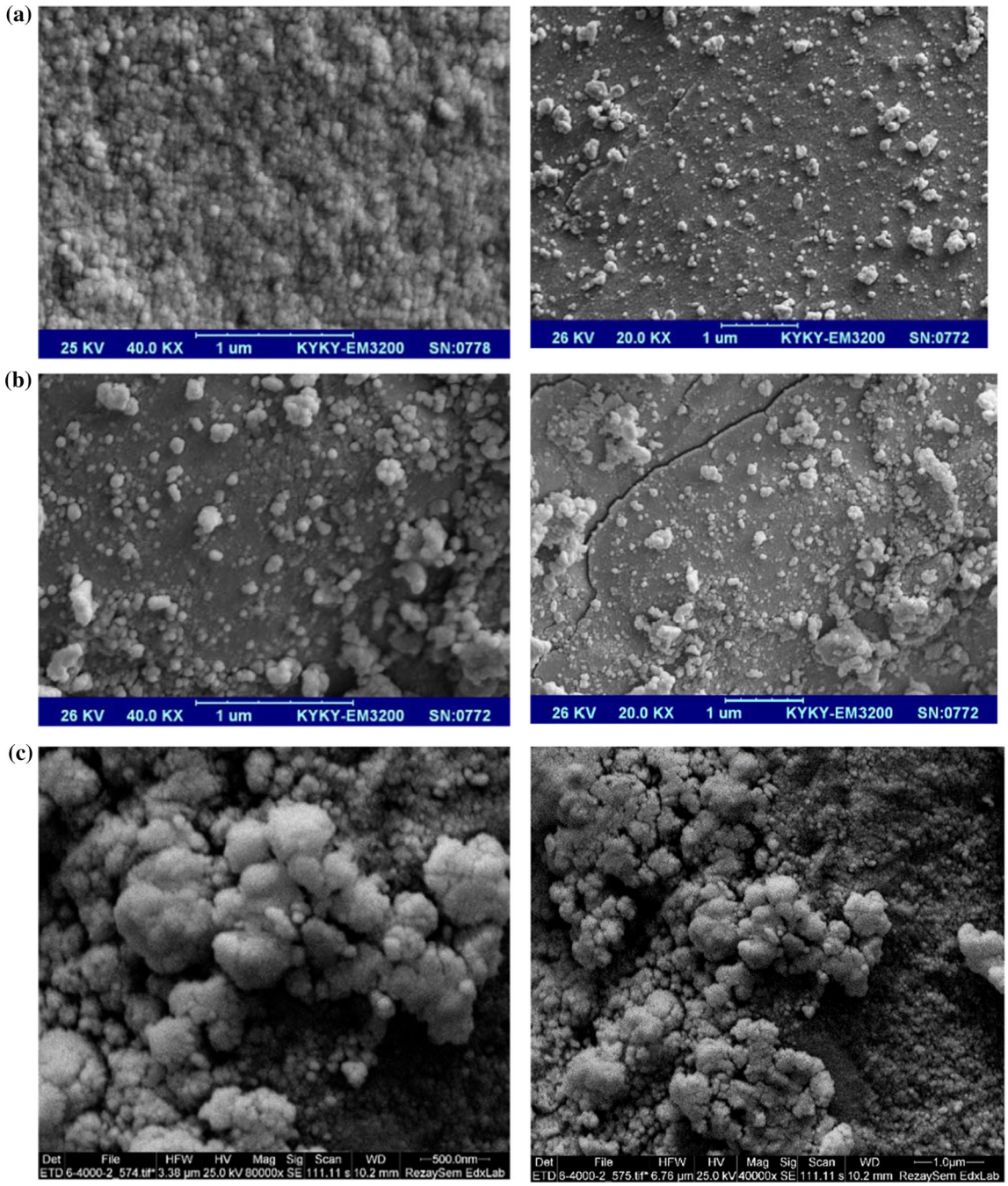

Fig. 7 SEM images of 58S-25 Mg bioactive nanocomposite at different resolutions **a** before, **b** after 14 days and **c** after 28 days of immersion in the SBF

Fig. 8. The peaks appeared in this figure at the approximate angles of 42° (101), 62° (103), 75° (004) and 79° (202) degrees are assigned to magnesium oxide nanoparticles (JCDPS No. 75- 0447) (Safaei-Ghomi et al. 2015), according to Fig. 9 in which the XRD pattern of purchasing MgO, presented by its manufacturer, is displayed. The XRD analysis of nanocomposites containing 58S bioactive glass and magnesium oxide nanoparticles shows that the synthesized samples exhibited glassy and amorphous structure, whereas the peaks confirming the presence of magnesium oxide were also noticeable. In addition, it is worth mentioning that the glassy and amorphous characteristics of these nanocomposites were not varied with an increase in the weight percent of magnesium oxide nanoparticles. On the other hand, it can be concluded that as the amount of magnesium oxide incorporated in the 58S-xMg nanocomposites increased, the intensity of the magnesium oxide's peaks enhanced, too.

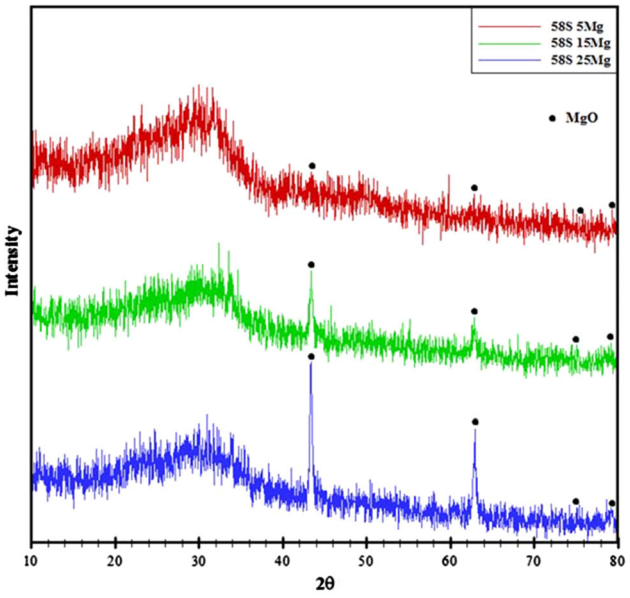

Fig. 8 XRD patterns of 58S-5 Mg (upper pattern), 58S-15 Mg (middle pattern) and 58S-25 Mg (down pattern) nanocomposites

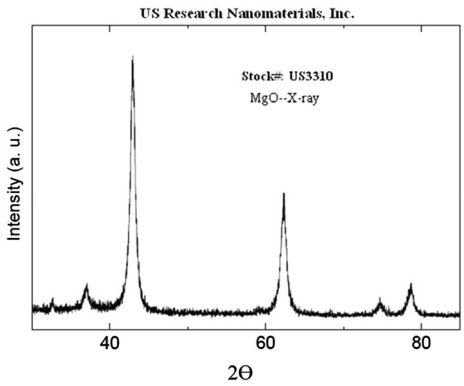

Fig. 9 XRD pattern of used MgO represented by its manufacturer

To evaluate the bioactivity of prepared nanocomposites, the X-ray diffraction patterns of the 58S-25 Mg sample before and after 14 (58S-25 Mg-14d) and 28 (58S-25 Mg-28d) days of immersion in the SBF solution are displayed in Fig. 10. The peaks corresponding to magnesium oxide and hydroxyapatite were specified in the patterns. According to the intensity of the hydroxyapatite peaks, it can be understood that 58S-25 Mg bioactive nanocomposite showed more bioactivity after 28 days of immersion in comparison with 14 days of immersion. The XRD pattern of the 58S-25 Mg-14d sample demonstrates that the hydroxyapatite peaks were formed beside the magnesium oxide peaks, although their intensity was lower than the intensity of magnesium oxide peaks. Tables 4 and 5 show details of XRD pattern for 58S 25 Mg-14d and 58S 25 Mg-28d samples, respectively.

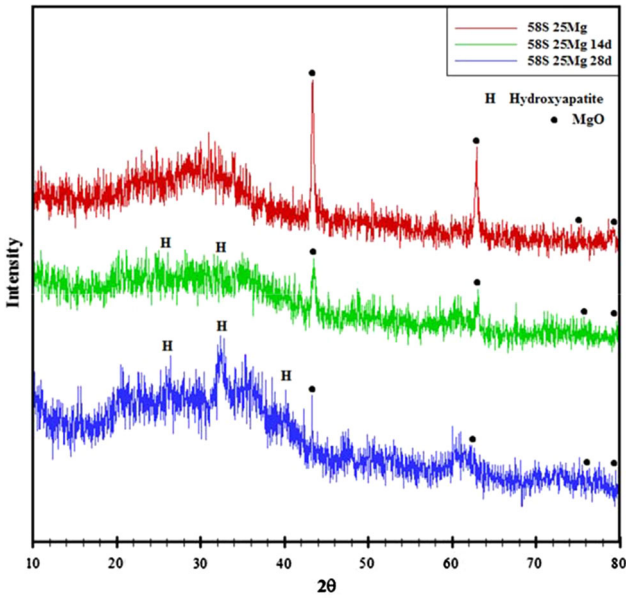

Fig. 10 XRD patterns of 58S-25 Mg bioactive glass nanocomposites (upper pattern), after 14 (middle pattern) and 28 days (down pattern) of immersion in the SBF solution

It is worth noting that this is not because the intensity of magnesium oxide peaks present in the 58S-25 Mg XRD pattern was changed after immersion in the SBF solution, but it also confirms that HA peaks emerged with approximately the same intensity as the existed MgO peaks. This issue can be observed in the XRD spectrum of the 58S-25 Mg sample after 28 days of immersion in the SBF solution, in which the intensity of the hydroxyapatite peaks (e.g., at 32°) increased to a level that the magnesium oxide peaks became less prominent in the pattern. So, based on these results, it is clear that the highest bioactivity was obtained for the 58S-25 Mg-28d sample since the peak of apatite diffraction became sharp and intense with a rise during the soaking time (Moghanian et al. 2018a).

Figure 11 illustrates the X-ray diffraction patterns of the 58S, 58S-5 Mg, 58S-15 Mg and 58S-25 Mg samples after 28 days of immersion in the simulated body fluid for the investigation of the MgO effect on the bioactivity of sol–gel-derived bioactive glasses. According to the intensity of hydroxyapatite peaks present in these XRD spectra, it is found that as the amount of magnesium oxide nanoparticles increased from 5 to 15 wt%, the bioactivity of the nanocomposites increased; however, as the amount of magnesium oxide incorporated in the nanocomposite increased from 15 to 25 wt%, the lower bioactive sample were obtained at the end of 28-day soaking. In other words, the 58S-15 Mg bioactive nanocomposite has higher bioactivity than the other two nanocomposites. Tables 6 and 7 show details of XRD pattern for 58S 15 Mg-28d and 58S 5 Mg-28d samples, respectively.

Table 4 Details of XRD pattern for bioactive materials phase – 58S 25 Mg-14d

Peak position 2θ (°)	FWHM Bsize (°)	d-spacing (A°)	Dp (nm)	Dp average (nm)
23.4	0.9	3.80963	9.422125023	6.472249429
30.6	0.9	2.92649	9.565381563	
35.19	2.2	2.55449	3.959664688	
39.6	3	2.27585	2.941826441	

Table 5 Details of XRD pattern for bioactive materials phase – 58S 25 Mg-28d

Peak position 2θ (°)	FWHM Bsize (°)	d-spacing (A°)	Dp (nm)	Dp average (nm)
26	0.7	3.38119	12.17449402	7.7
32.9	0.8	2.75569	9.620138772	
36.9	1.8	2.45452	4.863144557	
40	3	2.25522	2.945546089	

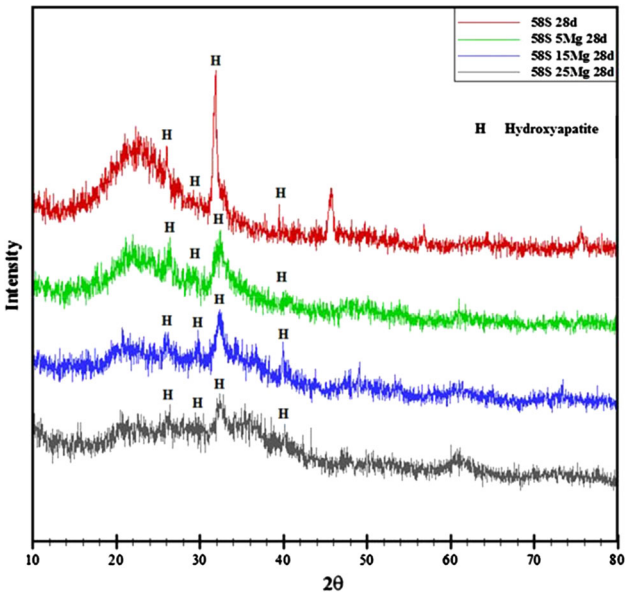

Fig. 11 XRD pattern of 58S (topest pattern), 58S-5 Mg (first middle pattern), 58S-15 Mg (second middle pattern) and 58S-25 Mg (down pattern) samples after 28 days of immersion in the SBF

A survey of the previous studies carried out in this area indicates that the similar results were acquired using a bioactive glass based on the CaO-MgO-P_2O_5-SiO_2 system which represented less bioactivity with an increase in the magnesium content from 5 to 20 mol% substituted for CaO (Essien et al. 2016). In another study, they also concluded that the apatite phase peaks were not observed for the glass sample with the highest MgO content (20% MgO). On the other hand, referring to these XRD patterns in this study, it is shown that even the nanocomposite prepared using 58S bioactive glass and the highest content of MgO nanoparticles (58S-25 Mg) showed the formation of hydroxyapatite on the nanocomposite surface (Ma et al. 2010a).

3.2.3 Functional Groups Analysis

A comparison of the FTIR spectra of 58S-5MgO, 58S-15 Mg and 58S-25 Mg samples before immersion in the SBF is presented in Fig. 12. As mentioned earlier, the peak at the wavenumber of 1090 cm-1 is related to asymmetric stretching bond Si–O–Si (Zhou et al. 2012). The main

Table 6 Details of XRD pattern for bioactive materials phase – 58S 15 Mg-28d

Peak position 2θ (°)	FWHM Bsize (°)	d-spacing (A°)	Dp (nm)	Dp average (nm)
26.17289	0.7	3.40494	12.17875002	8.635499352
30.10946	0.6	2.96814	14.33142038	
32.27457	1.7	2.7738	5.084895979	
40.1477	3	2.24615	2.946931032	

Table 7 details of XRD pattern for bioactive materials phase – 58S 15 Mg-28d

Peak position 2θ (°)	FWHM Bsize (°)	d-spacing (A°)	Dp (nm)	Dp average (nm)
26.3	0.6	3.38585	14.21221508	6.295339012
32.4	1.8	2.76294	4.803926072	
35.2	2.8	2.55451	3.111251225	
40.7	2.9	2.21819	3.053963666	

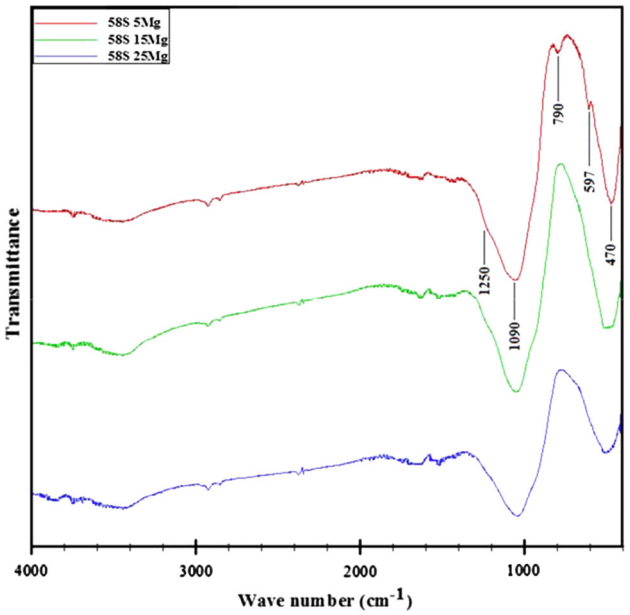

Fig. 12 FTIR spectra of 58S-5 Mg (upper pattern), 58S-15 Mg (middle pattern) and 58S-25 Mg (down pattern) samples before immersion in the SBF

absorption band obtained at 1250 cm-1 can be assigned to the asymmetric stretching of Si–O–Si (Moghanian et al. 2018b). On the other hand, the peaks in the wavenumber range between 440 and 900 cm ^{1} may be related to the stretching bond of Mg-O (Jeon et al. 2012; Ma et al. 2011a; Nassar et al. 2017).

Figure 13 shows the FTIR spectrum of the 58S-25 Mg sample before and after immersion in the SBF for 14 and 28 days. The main peaks seen in the XRD pattern of the 58S-25 Mg sample before immersion are described in Fig. 12. In this section, the comparison of the peaks observed in the FTIR spectra of 58S-25 Mg before and after soaking in the SBF solution is discussed. Two new peaks are observed in the FTIR spectra of 58S-25 Mg after soaking at about 1630 and 3440 cm^{-1} which can be ascribed to the O–H bond due to the water presence. This may be due to the presence of groups such as P-OH or Ca-OH, which result in moisture absorption (Mami et al. 2008). The peaks appeared in the range of 1400 to 1500 cm^{-1} are related to the C–O bond, which represents the formation of hydroxycarbonate apatite (HCA) layer on the surface of nanocomposite samples. (Essien et al. 2016) Another new peak, which is observed at the wavenumber of 603 cm^{-1}, indicates the presence of the PO_4 bond in the apatite network (Taghian Dehaghani et al. 2015). Also, the peak at the wavenumber of about 870 cm^{-1} is attributed to the C–O bond in the carbonate groups in phosphate groups in the apatite network (Rainer et al. 2008; Zhao et al. 2011). As can be seen, the peak at 1090 cm^{-1} became sharper after immersion in the SBF, which could be due to the destruction of the Si–O–Si network to form hydroxyapatite. Therefore, it can be concluded that as the intensity of this peak enhanced, more hydroxyapatite was formed on the nanocomposite surface (Ji et al. 2017).

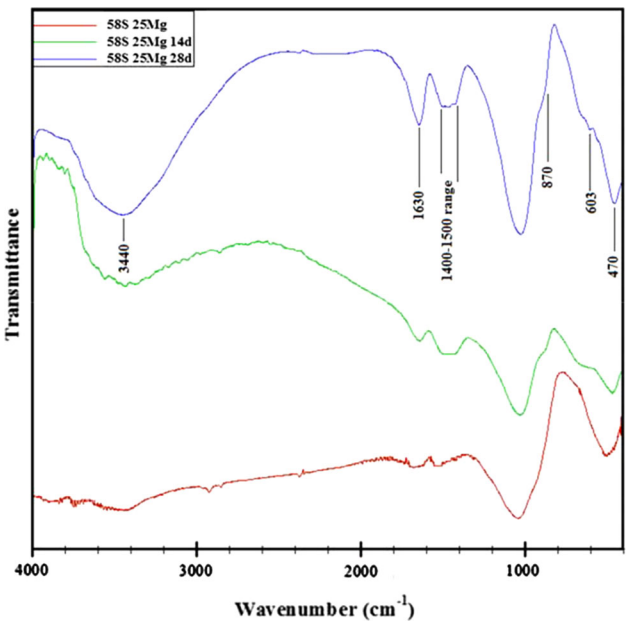

Fig. 13 FTIR spectra of 58S-25 Mg bioactive glass nanocomposite (upper pattern) after 14 (middle pattern) and 28 days (down pattern) of immersion in the SBF solution

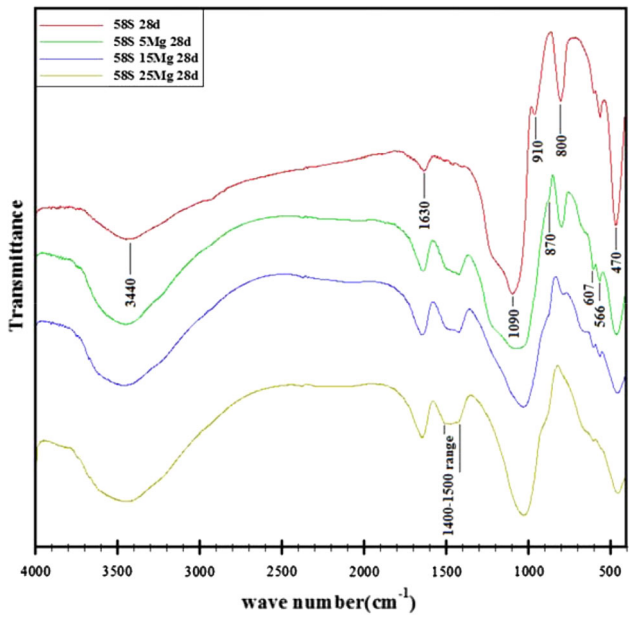

Fig. 14 FTIR spectra of 58S (topest pattern), 58S-5 Mg (first middle pattern), 58S-15 Mg (second middle pattern) and 58S-25 Mg (down pattern) bioactive glass nanocomposites after 28 days of immersion in the SBF

Figure 14 shows the FTIR spectra of 58S, 58S-5 Mg, 58S-15 Mg and 58S-25 Mg samples after immersion in the SBF for 28 days. The comparison of these FTIR patterns is a good way to evaluate the bioactivity of nanocomposites containing various weight percent of magnesium. The specified peaks in this figure were described in the previous sections. As mentioned before, the formation of the crystalline apatite layer on the surface of the nanocomposite samples is verified due to the P-O vibrating bonds appeared at the wavenumbers of 566 cm^{-1} and 607 cm^{-1} (Taghian Dehaghani et al. 2015). Also, peaks observed around wavenumber of 1392–1435 cm^{-1} range assure the presence of carbonate group into the apatite layer (Singh et al. 2019).

From the above description, it can be concluded that 58S bioactive glass exhibited high bioactive property compared to other samples (58S-5 Mg, 58S-15 Mg and 58S-25 Mg) at end of 28 day soaking in SBF solution. It can be attributed to the different porosity of the 58S bioactive glass and synthesized nanocomposites. Higher porosity supplies more sites for precipitation. Another reason for this result can be at attribute to many factors like, the speed and manner of the migration of Ca^{2+} and PO_4^{3-} groups to the surface forming $CaO\backslash PO_4^{3-}$ clusters on the top of the SiO_2-rich layer was done, followed by growth of the amorphous CaP, after that, the crystallization of the amorphous CaP (Polymeris et al. 2017). Also, it can be concluded that 58S-15 Mg sample has exhibited higher bioactivity in comparison to the other nanocomposite of BGs, by investigating both, FTIR spectra and XRD patterns of the samples. A similar consequence has been concluded by Moghanian et al. They reported that the presence of magnesium in 58S bioactive glass increased bioactivity of BGs first, after that by adding more magnesium to 58S bioactive glass, the bioactivity of sample decreased (Moghanian et al. 2018b).

3.2.4 Antibacterial Test

Figure 15 presents the comparative study of the antibacterial activity of synthesized bioactive nanocomposites against MRSA bacteria. According to the obtained values for bactericidal activity, 58S-15 Mg possessed higher bactericidal efficiency against MRSA bacteria than 58S-5 Mg and 58S-25 Mg while showing lower bactericidal efficiency compared to 58S nanobioactive glass. These results revealed that MgO exhibited remarkable dose-dependent antibacterial activity against MRSA bacteria, i.e., by increasing the amount of MgO substituted in bioactive nanocomposite from 5 to 15 wt%, its bactericidal efficiency significantly increased. However, the sample with the 25 weight percent MgO had a reverse effect and led to a significant decrease in the bactericidal efficiency than the

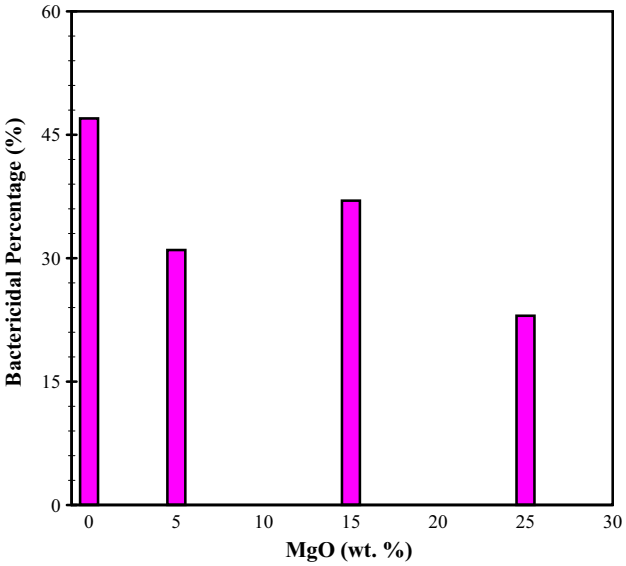

Fig. 15 Antibacterial activity of 58S, 58S-5 Mg, 58S-15 Mg and 58S-25 Mg bioactive glass nanocomposites

58S-15 Mg. It must be noted that many factors are related to antibacterial activities of bioactive glass (like the presence of ions such as phosphate, calcium and magnesium), but the precise mechanism of it is not discovered yet (Moghanian et al. 2019). In brief, for the present study among the synthesized nanocomposites, the 58S-15 Mg sample exhibited the highest antibacterial activity of 37.5%.

4 Conclusions

This research focused on the application of direct impregnation of MgO nanoparticles as a base precursor in the preparation of bioactive glasses with no change in the 58S composition, although previous studies reported the usage of MgO sources like $Mg(NO_3)_2.6H_2O$ substituted for one of the routine precursors of 58S bioglass. Novel bioactive glass–magnesium oxide nanocomposites by directly adding different weight percent of magnesium oxide nanoparticles to 58S bioactive glass material were successfully synthesized by the sol–gel method. Then, the effect of MgO nanoparticles content present in the nanocomposites was investigated on the bioactivity of nanocomposite powders through the immersion of the samples in the simulated body fluid (SBF) at different time intervals of 14 and 28 days. Moreover, the antibacterial activity of the produced nanocomposites against MRSA bacteria was studied. The results are as follows:

1. Amorphous and glassy nature of the synthesized samples (58S, 58S-5 Mg, 58S-15 Mg and 58S-25 Mg) was verified by their XRD patterns.

2. According to the XRD patterns and the FTIR spectra of the samples after soaking in the SBF solution, 58S, 58S-5 Mg, 58S-15 Mg and 58S-25 Mg were bioactive materials due to the formation of hydroxyapatite on their surface.
3. The XRD results also confirmed that the bioactivity of nanocomposites first increased with an increase in the content of magnesium oxide nanoparticles up to 15 wt% and then decreased as the weight percent of MgO nanoparticles changed from 15 to 25 wt%.
4. The antibacterial activity assessment showed that 58S-15 Mg had more antibacterial activity than two other nanocomposites containing magnesium oxide nanoparticles.

References

Abdalla MM, Lung CYK, Neelakantan P, Matinlinna JP (2020) A novel, doped calcium silicate bioceramic synthesized by sol–gel method: Investigation of setting time and biological properties. J Biomed Mater Res B 108:56–66

Aguiar H et al (2008) Orthophosphate nanostructures in SiO2–P2O5–CaO–Na2O–MgO bioactive glasses. J Non Cryst Solids 354:4075–4080

Anand V, Singh K, Kaur K (2014) Evaluation of zinc and magnesium doped 45S5 mesoporous bioactive glass system for the growth of hydroxyl apatite layer. J Non Cryst Solids 406:88–94

Bellucci D, Sola A, Salvatori R, Anesi A, Chiarini L, Cannillo V (2017) Role of magnesium oxide and strontium oxide as modifiers in silicate-based bioactive glasses: Effects on thermal behaviour, mechanical properties and in-vitro bioactivity. Mater Sci Eng C 72:566–575

Bohner M, Lemaitre J (2009) Can bioactivity be tested in vitro with SBF solution? Biomaterials 30:2175–2179

Cole KA, Funk GA, Rahaman MN, McIff TE (2019) Characterization of the conversion of bone cement and borate bioactive glass composites. J Biomed Mater Res B

Deng J, Li P, Gao C, Feng P, Shuai C, Peng S (2014) Bioactivity improvement of forsterite-based scaffolds with nano-58S bioactive glass. Mater Manuf Process 29:877–884

dos Santos DM, de Carvalho SM, Pereira MM, Houmard M, Nunes EH (2019) Freeze-cast composite scaffolds prepared from sol-gel derived 58S bioactive glass and polycaprolactone. Ceram Int 45:9891–9900

Essien ER, Atasie VN, Udobang EU (2016) Microwave energy-assisted formation of bioactive CaO–MgO–SiO 2 ternary glass from bio-wastes. Bull Mater Sci 39:989–995

Farano V, Maurin JC, Attik N, Jackson P, Grosgogeat B, Gritsch K (2019) Sol–gel bioglasses in dental and periodontal regeneration: a systematic review. J Biomed Mater Res B 107:1210–1227

Feyerabend F, Witte F, Kammal M, Willumeit R (2006) Unphysiologically high magnesium concentrations support chondrocyte proliferation and redifferentiation. Tissue Eng 12:3545–3556

Gu Y, Zhang J, Zhang X, Liang G, Xu T, Niu W (2019) Three-dimensional printed Mg-Doped β-TCP bone tissue engineering scaffolds: effects of magnesium ion concentration on Osteogenesis and Angiogenesis in vitro tissue. Eng Regen Med 16:415–429

Hong Y, Wang Y, Li B, Pan G (2019) Immobilizing nitrifying bacteria with Fe2O3-CaO-SiO2 porous glass-ceramics. Int J Appl Glass Sci 10:228–234

Hoo CM, Starostin N, West P, Mecartney ML (2008) A comparison of atomic force microscopy (AFM) and dynamic light scattering (DLS) methods to characterize nanoparticle size distributions. J Nanopart Res 10:89–96

Huang K et al (2014) Sol–gel derived mesoporous 58S bioactive glass coatings on AZ31 magnesium alloy and in vitro degradation behavior. Surf Coat Technol 240:137–144

Huang C-L, Fang W, Chen I-H, Hung T-Y (2018) Manufacture and biomimetic mineral deposition of nanoscale bioactive glasses with mesoporous structures using sol-gel methods. Ceram Int 44:17224–17229

Jeon H, Min YJ, Ahn SH, Hong S-M, Shin J-S, Kim JH, Lee KB (2012) Graft copolymer templated synthesis of mesoporous MgO/TiO2 mixed oxide nanoparticles and their CO2 adsorption capacities Colloids. Surf A Physicochem Eng Asp 414:75–81

Ji L et al (2017) Synthesis of nanosized 58S bioactive glass particles by a three-dimensional ordered macroporous carbon template. Mater Sci Eng C 75:590–595

Kaur K, Singh K, Anand V, Bhatia G, Singh S, Kaur H, Arora DS (2016) Magnesium and silver doped CaO–Na2O–SiO2–P2O5 bioceramic nanoparticles as implant materials. Ceram Int 42:12651–12662

Kaur G, Pickrell G, Sriranganathan N, Kumar V, Homa D (2016) Review and the state of the art: sol–gel and melt quenched bioactive glasses for tissue engineering. J Biomed Mater Res B 104:1248–1275

Li R, Clark A, Hench L (1991) An investigation of bioactive glass powders by sol-gel processing. J Appl Biomater Func 2:231–239

Li H, Wang D, Hu J, Chen C (2013) Effect of the partial substitution of K2O, MgO, B2O3 for CaO on crystallization, structure and properties of Na2O–CaO–SiO2–P2O5 system glass-ceramics. Mater Lett 106:373–376

Liu Y-J, Su W-T, Chen P-H (2018) Magnesium and zinc borate enhance osteoblastic differentiation of stem cells from human exfoliated deciduous teeth in vitro. J Biomater Appl 32:765–774

Lucas-Girot A, Mezahi FZ, Mami M, Oudadesse H, Harabi A, Le Floch M (2011) Sol–gel synthesis of a new composition of bioactive glass in the quaternary system SiO2–CaO–Na2O–P2O5: comparison with melting method. J Non Cryst Solids 357:3322–3327

Ma J, Chen C, Wang D, Jiao Y, Shi J (2010) Effect of magnesia on the degradability and bioactivity of sol–gel derived SiO2–CaO–MgO–P2O5 system glasses. Colloids Surf B Biointerfaces 81:87–95

Ma J, Chen C, Wang D, Meng X, Shi J (2010) In vitro degradability and bioactivity of mesoporous CaO-MgO-P 2 O 5-SiO 2 glasses synthesized by sol–gel method. J Solgel Sci Technol 54:69–76

Ma J, Chen C, Wang D, Hu J (2011) Effect of magnesia on structure, degradability and in vitro bioactivity of CaO–MgO–P2O5–SiO2 system ceramics. Mater Lett 65:130–133

Ma J, Chen C, Wang D, Hu J (2011) Synthesis, characterization and in vitro bioactivity of magnesium-doped sol–gel glass and glass-ceramics. Ceram Int 37:1637–1644

Mami M, Lucas-Girot A, Oudadesse H, Dorbez-Sridi R, Mezahi F, Dietrich E (2008) Investigation of the surface reactivity of a sol–gel derived glass in the ternary system SiO2–CaO–P2O5. Appl Surf Sci 254:7386–7393

Moghanian A et al. (2019) Novel antibacterial Cu/Mg-substituted 58S-bioglass: Synthesis, characterization and investigation of in vitro bioactivity. Int J Appl Glass Sci

Moghanian A, Sedghi A, Ghorbanoghli A, Salari E (2018) The effect of magnesium content on in vitro bioactivity, biological behavior

and antibacterial activity of sol–gel derived 58S bioactive glass. Ceram Int 44:9422–9432
Moghanian A, Firoozi S, Tahriri M, Sedghi A (2018) A comparative study on the in vitro formation of hydroxyapatite, cytotoxicity and antibacterial activity of 58S bioactive glass substituted by Li and Sr. Mater Sci Eng C 91:349–360
Mohammadkhah A, Day DE (2018) Mechanical properties of bioactive glass/polymer composite scaffolds for repairing load bearing bones. Int J Appl Glas Sci 9:188–197
Mokhtari H, Ghasemi Z, Kharaziha M, Karimzadeh F, Alihosseini F (2018) Chitosan-58S bioactive glass nanocomposite coatings on TiO2 nanotube: Structural and biological properties. Appl Surf Sci 441:138–149
Nabian N, Jahanshahi M, Rabiee SM (2011) Synthesis of nano-bioactive glass–ceramic powders and its in vitro bioactivity study in bovine serum albumin protein. J Mol Struct 998:37–41
Nabian N, Delavar M, Rabiee MS, Jahanshahi M (2013) Quenched/unquenched nanobioactive glass-ceramics: Synthesis and in vitro bioactivity evaluation in Ringer's solution with BSA. Chem Ind Chem Eng Q 19:231–239
Nassar MY, Mohamed TY, Ahmed IS, Samir I (2017) MgO nanostructure via a sol-gel combustion synthesis method using different fuels: an efficient nano-adsorbent for the removal of some anionic textile dyes. J Mol Liq 225:730–740
Pérez-Pariente J, Balas F, Vallet-Regi M (2000) Surface and Chemical Study of SiO2⊙ P2O5⊙ CaO⊙(MgO) Bioactive Glasses. Chemistry of materials 12:750–755
Polymeris G et al (2017) Bioactivity characterization of 45S5 bioglass using TL, OSL and EPR: comparison with the case of 58S sol-gel bioactive glass. Mater Sci Eng C 70:673–680
Prabhu M, Kavitha K, Manivasakan P, Rajendran V, Kulandaivelu P (2013) Synthesis, characterization and biological response of magnesium-substituted nanobioactive glass particles for biomedical applications. Ceram Int 39:1683–1694
Rabiee SM, Nazparvar N, Azizian M, Vashaee D, Tayebi L (2015) Effect of ion substitution on properties of bioactive glasses: A review. Ceram Int 41:7241–7251
Rabiee SM, Nazparvar N, Rajabi M (2018) Structural behavior and in vitro bioactivity evaluation of Sol-Gel derived glass-ceramics based on SiO 2-CaO-P 2 O 5-ZnO system. Silicon 10:67–75
Rainer A, Giannitelli SM, Abbruzzese F, Traversa E, Licoccia S, Trombetta M (2008) Fabrication of bioactive glass–ceramic foams mimicking human bone portions for regenerative medicine. Acta Biomater 4:362–369
Saboori A, Sheikhi M, Moztarzadeh F, Rabiee M, Hesaraki S, Tahriri M, Nezafati N (2009) Sol-gel preparation, characterisation and in vitro bioactivity of Mg containing bioactive glass. Ads Appl Ceram 108:155
Safaei-Ghomi J, Zahedi S, Javid M, Ghasemzadeh MA (2015) MgO nanoparticles: an efficient, green and reusable catalyst for the one- pot syntheses of 2,6-Dicyanoanilines and 1,3-Diarylpropyl Malononitriles under different conditions. J Nanostruct 5:153–160
Saqaei M, Fathi M, Edris H, Mortazavi V, Hosseini N (2016) Effects of adding forsterite bioceramic on in vitro activity and antibacterial properties of bioactive glass-forsterite nanocomposite powders. Adv Powder Technol 27:1922–1932
Saravanakumar B, Prabhu M, Rajendran V, Gopal J, Mudali UK (2015) Electrochemical deposition of 58SiO2-33CaO-9P2O5 nanobioactive glass particles on Ti-6Al-4V alloy for biomedical applications. Int J Appl Ceram Technol 12:95–105
Sawai J (2003) Quantitative evaluation of antibacterial activities of metallic oxide powders (ZnO, MgO and CaO) by conductimetric assay. J Microbiol Methods 54:177–182
Seuss S, Lehmann M, Boccaccini AR (2014) Alternating current electrophoretic deposition of antibacterial bioactive glass-chitosan composite coatings. Int J Mol Sci 15:12231–12242
Shih S-J, Chou Y-J, Chien I-C (2012) One-step synthesis of bioactive glass by spray pyrolysis. J Nanopart Res 14:1299
Shih S-J, Chou Y-J, Borisenko KB (2013) Preparation method: Structure–bioactivity correlation in mesoporous bioactive glass. J Nanopart Res 15:1763
Singh AK, Pramanik K, Biswas A (2019) MgO enables enhanced bioactivity and antimicrobial activity of nano bioglass for bone tissue engineering application. Mater Technol 34:818–826
Strobel L et al (2013) Novel strontium-doped bioactive glass nanoparticles enhance proliferation and osteogenic differentiation of human bone marrow stromal cells. J Nanopart Res 15:1780
Sukhorukova I, Sheveyko A, Kiryukhantsev-Korneev PV, Levashov E, Shtansky D (2017) In vitro bioactivity study of TiCaPCO (N) and Ag-doped TiCaPCO (N) films in simulated body fluid. J Biomed Mater Res B 105:193–203
Sun Y, Devore D, Ma X, Yuan Y, Kohn J, Qian J (2019) Promotion of dispersion and anticancer efficacy of hydroxyapatite nanoparticles by the adsorption of fetal bovine serum. J Nanopart Res 21:267
Taghian Dehaghani M, Ahmadian M, Fathi M (2015) Synthesis, characterization, and bioactivity evaluation of amorphous and crystallized 58S bioglass nanopowders. Int J Appl Ceram Technol 12:867–874
Taherian M, Rojaee R, Fathi M, Tamizifar M (2014) Effect of different sol-gel synthesis processes on microstructural and morphological characteristics of hydroxyapatite-bioactive glass composite nanopowders. J Adv Ceram 3:207–214
Wang L et al (2020) Effect of nanoscale bioactive glass with radial spherical particles on osteogenic differentiation of rat bone marrow mesenchymal stem cells. J Mater Sci Mater Med 31:1–11
Ye K et al (2019) Three-dimensional electrospun nanofibrous scaffolds displaying bone morphogenetic protein-2-derived peptides for the promotion of osteogenic differentiation of stem cells and bone regeneration. J Colloid Interf SCI 534:625–636
Yoshizawa S, Brown A, Barchowsky A, Sfeir C (2014) Magnesium ion stimulation of bone marrow stromal cells enhances osteogenic activity, simulating the effect of magnesium alloy degradation. Acta Biomater 10:2834–2842
Zhao X et al (2011) vitro assessment of cellular responses to rod-shaped hydroxyapatite nanoparticles of varying lengths and surface areas. Nanotoxicology 5:182–194
Zhou Y, Li H, Lin K, Zhai W, Gu W, Chang J (2012) Effect of heat treatment on the properties of SiO 2–CaO–MgO–P 2 O 5 bioactive glasses. J Mater Sci Mater Med 23:2101–2108